Nano Research 2014, 7(9): 1319–1326
DOI 10.1007/s12274-014-0496-x
Research Article
ISSN 1998-0124
CN 11-5974/O4

SnO_2–reduced graphene oxide nanoribbons as anodes for lithium ion batteries with enhanced cycling stability

Lei Li[1,§], Anton Kovalchuk[1,§], and James M. Tour[1,2,3] (✉)

[1] *Department of Chemistry, Rice University, 6100 Main Street, Houston, Texas 77005, USA*
[2] *Richard E. Smalley Institute for Nanoscale Science and Technology, Rice University, 6100 Main Street, Houston, Texas 77005, USA*
[3] *Department of Materials Science and NanoEngineering, Rice University, 6100 Main Street, Houston, Texas 77005, USA*
[§] *The authors contributed equally to this work.*

Received: 26 March 2014
Revised: 8 May 2014
Accepted: 12 May 2014

KEYWORDS
lithium ion battery,
tin oxide,
graphene oxide nanoribbons,
energy storage

ABSTRACT

A nanocomposite material of SnO_2–reduced graphene oxide nanoribbons has been developed. In this composite, the reduced graphene oxide nanoribbons are uniformly coated by nanosized SnO_2 that formed a thin layer of SnO_2 on the surface. When used as anodes in lithium ion batteries, the composite shows outstanding electrochemical performance with the high reversible discharge capacity of 1,027 mAh/g at 0.1 A/g after 165 cycles and 640 mAh/g at 3.0 A/g after 160 cycles with current rates varying from 0.1 to 3.0 A/g and no capacity decay after 600 cycles compared to the second cycle at a current density of 1.0 A/g. The high reversible capacity, good rate performance and excellent cycling stability of the composite are due to the synergistic combination of electrically conductive reduced graphene oxide nanoribbons and SnO_2. The method developed here is practical for the large-scale development of anode materials for lithium ion batteries.

1 Introduction

The electrochemical storage of energy using lithium ion batteries (LIBs) is a most effective and practical technology [1, 2]. LIBs need high power and energy density with excellent performance during cycling to meet critically important needs of growing applications in electric vehicles, multifunctional electrical devices and communications equipment. LIBs will also be important in storing the energy produced using renewable energy sources since such sources may be far from existing electrical grids [3, 4]. The development of better electrode materials has been the subject of extensive research [1, 3, 5]. Tin oxide (SnO_2) has attracted attention because it has a theoretical reversible capacity of ~790 mAh/g, which is almost twice that of anodes based on graphite [6, 7]. However, the reversible charging and discharging process is accompanied by a large volume variation. The volume change can result in the pulverization of SnO_2 and the loss of electrical contact. This causes a rapid capacity decay upon extended cycling [6, 8]. Therefore, the development

Address correspondence to tour@rice.edu

of SnO_2-based anodes with enhanced cycling stability and high capacity is becoming important.

Research based on different strategies for improvement of SnO_2-based anodes has been reported. One approach is to prepare SnO_2-based composites using different carbon materials, such as amorphous carbon [8–11], graphene [12–16], carbon nanotubes [17–19] and graphene nanoribbons [20]. The carbon materials not only mitigate the volume variation, but also improve the electrical conductivity of the composites. Another approach is the use of nanostructured SnO_2 such as nanotubes [21, 22], nanowires [23] and nanosheets [24], to buffer the volume variation. At the same time, the nanostructures can improve the kinetic properties of the electrode materials, stabilize the solid electrolyte interface (SEI), and improve the rate performance [8, 25]. Preparation of SnO_2 composites with other matrix elements or metal oxides and control of the proper voltage range of the batteries can also help to reduce the adverse effects caused by the volume changes [16, 17, 26–28]. These strategies have resulted in improvements in the electrochemical performance of SnO_2-based anode materials. However, the cycling stability of the SnO_2-based anode materials has not been similarly improved. Therefore, the preparation of high capacity SnO_2-based anode materials with improved cycling stability remains a challenge worth pursuing.

In this study, we developed a facile strategy to fabricate SnO_2–reduced graphene oxide nanoribbons (SnO_2–rGONRs)—which have the merits of both SnO_2 nanostructures and carbon materials—with the aim of improving energy storage in LIBs, especially the cycling performance. The synthesis of graphene oxide nanoribbons (GONRs) is scalable and GONRs have a high surface area, making them suitable templates on which to directly grow SnO_2 nanoparticles without aggregation using a wet chemistry process in water to form the SnO_2–GONRs [29, 30]. SnO_2–rGONRs were produced by reduction with hydrazine [31]. rGONRs maintain contact with the SnO_2 nanoparticles, producing good electrical conductivity of the SnO_2–rGONRs. More importantly, rGONRs improve the electrochemical stability characteristics of the composite, thereby buffering volume changes, and thus the non-aggregated, nanosized SnO_2 particles effectively relieve volume change stress due to their high surface area. What is more, the nanosized structure can reduce the diffusion path length of the metal particles that are formed through the alloying–dealloying process, increasing the concentration of Li ions in the active materials, leading to the enhancement of the anode kinetic and current rate capabilities [25]. SnO_2–rGONRs as anode materials demonstrate high capacity, good rate performance, and excellent cycling operation. The reversible discharge capacity was 640 mAh/g at 3.0 A/g after 160 cycles and 1,027 mAh/g at 0.1 A/g after 165 cycles with current rates varying from 0.1 to 3.0 A/g. The discharge capacity showed no decay and increased about 2.2% after 600 cycles compared to the second cycle at a current density of 1.0 A/g. Based on these data, SnO_2–rGONRs are superb candidates for use as anode materials with great cycling stability in LIBs.

2 Results and discussion

The preparation of SnO_2–rGONRs is shown in Scheme 1. Unzipping of multiwalled carbon nanotubes (MWCNTs) using solution chemistry was used to prepare the GONRs. Then, SnO_2–GONRs were obtained through the reaction between $SnCl_2$ and NaOH in the presence of GONRs in ethylene glycol. Finally, SnO_2–rGONRs were obtained by hydrazine reduction. In order to study the morphology of SnO_2–rGONRs, rGONRs were also prepared in the same way as SnO_2–rGONRs.

The structure of the SnO_2–rGONRs and rGONRs was characterized by transmission electron microscopy

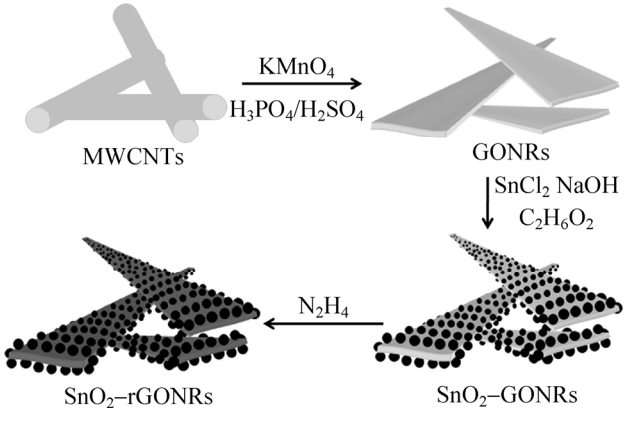

Scheme 1 Schematic illustration of the synthesis of SnO_2–rGONRs.

(TEM) and scanning electron microscopy (SEM). Figure S1 (in the Electronic Supplementary Material (ESM)) shows the morphology of rGONRs, which have a width of ~300 nm and length of ~8 μm. Figures 1(a) and 1(b) depict the structure of SnO_2–rGONRs at various magnifications. Nanosized SnO_2 particles homogeneously grow on the surface of rGONRs. The high resolution TEM images of SnO_2–rGONRs in Figs. 1(c) and 1(d) demonstrate that the synthesized SnO_2 were nanosized particles, which formed a thin surface layer on rGONRs.

The composites were also characterized by X-ray diffraction (XRD) and X-ray photoelectron spectroscopy (XPS). The XRD patterns of rGONRs and SnO_2–rGONRs are shown in Fig. 2(a). The pattern of rGONRs showed the characteristic (002) diffraction peak of graphite centered at 24.6°[32]. This peak was absent in the pattern of SnO_2–rGONRs because SnO_2 nanoparticles covered the surface of the rGONRs and the strong XRD peaks of SnO_2 overlapped those of the rGONRs. Figure S2 (in the ESM) shows the XRD peaks of SnO_2–GONRs, which, when combined with Fig. 2(a), shows that SnO_2 was stable after the reduction of GONRs. Figure 2(b) is the survey XPS spectrum of composite SnO_2–rGONRs. It can be seen that SnO_2–rGONRs only contained Sn, C, O, and trace amounts of N, the last probably arising from the hydrazine. Moreover, Sn $3d_{3/2}$ and Sn $3d_{5/2}$ peaks were detected in the fine spectrum of Sn 3d, confirming the formation of SnO_2-containing SnO_2–rGONRs (Fig. 2(c)). Figure 2(d) shows the fine XPS C1s spectrum of SnO_2–rGONRs, which was deconvoluted into five peaks located at 284.5, 285.5, 286.4, 287.6, and 289.1 eV, which can be assigned to C=C (sp^2 C), C–C (sp^3 C), C–O, C=O and O–C=O, respectively [29, 32, 33]. The low concentration of oxidized carbon in the SnO_2–rGONRs suggests that the GONRs were almost completely reduced by hydrazine [29, 32]. The data demonstrate that SnO_2 nanoparticles are indeed grown on the rGONRs. TGA curve shows the SnO_2 content in the composite is 70%, as measured by heating in air at a rate of 5 °C/min (Fig. S3 in the ESM).

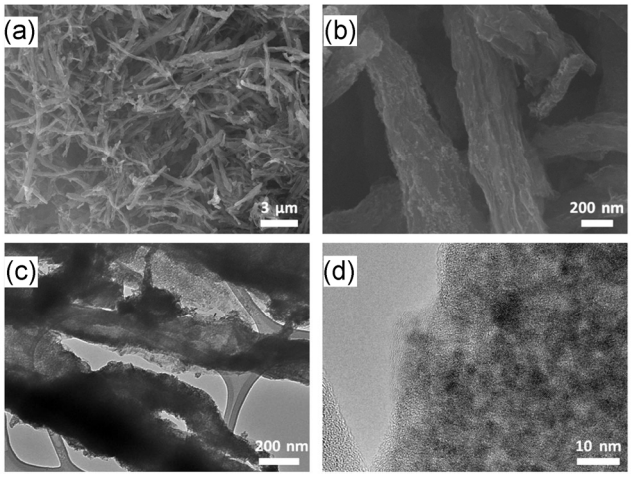

Figure 1 (a) and (b) SEM images of SnO_2–rGONRs at different resolutions. (c) and (d) TEM images of SnO_2–rGONRs at different resolutions.

The electrochemical performance of SnO_2–rGONRs as anodes in LIBs was tested by cyclic voltammetry (CV). Figure 3(a) shows the first two cycles of CV. In the first discharge cycle, there are three cathodic peaks centered at 1.3, 0.8, and 0.06 V. The peak at 1.3 V results from the reduction of SnO_2 to SnO and the formation of Li_2O; the broad cathodic peaks at ~0.8 V result from the reduction of SnO_2 to Sn and Li_2O, SnO to Sn, and the formation of a SEI; the peak at 0.06 V results from the alloying of Sn and Li and the intercalation of lithium ions into the rGONRs. At the same time, there are two anodic peaks at 0.57 and 1.26 V. The former peak results from the dealloying of Sn and Li, and the other peak results from the partial conversion of Sn to SnO_2 and SnO [8, 34]. In the second cycle, the broad peak at 0.8 V disappears and a new peak appears at 0.96 V. This demonstrates that the formation of the SEI mainly occurs in the first cycle and the new peak results from the peak shift of the reduction reaction of SnO_2 [8]. The CV curves mostly overlap, indicating the good reversibility of the electrochemical reaction. In the first two discharge–charge profiles, two plateaus in the discharging and charging processes are consistent with the CV data. In addition, the first discharge capacity of SnO_2–rGONRs is higher than the theoretical capacity, which might result from decomposition of electrolyte, irreversible electrode reactions and/or the surface formation of SEI on the electrodes [8, 34].

The rate characteristics of the SnO_2–rGONRs were evaluated in the same potential window as indicated in Fig. 4(a). Stable capacities were observed at different current densities from 0.1 to 3 A/g. At a current density

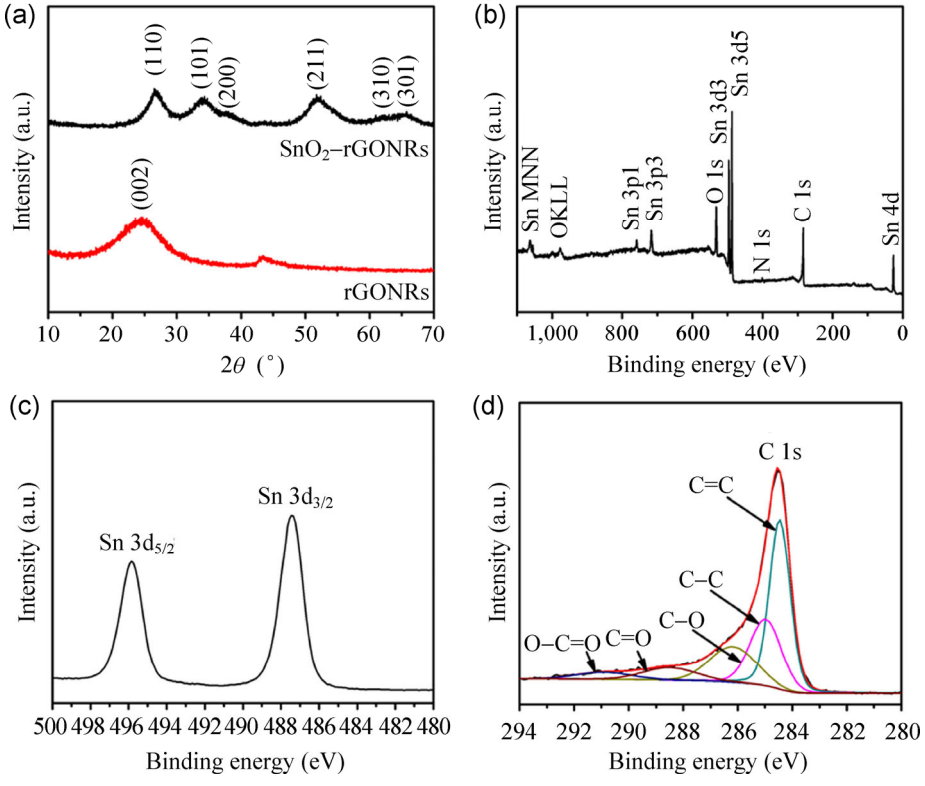

Figure 2 (a) XRD patterns of SnO_2–rGONRs and rGONRs. (b) XPS survey spectrum of SnO_2–rGONRs. (c) Sn 3d XPS spectrum of SnO_2–rGONRs. (d) C1s XPS spectrum of SnO_2–rGONRs.

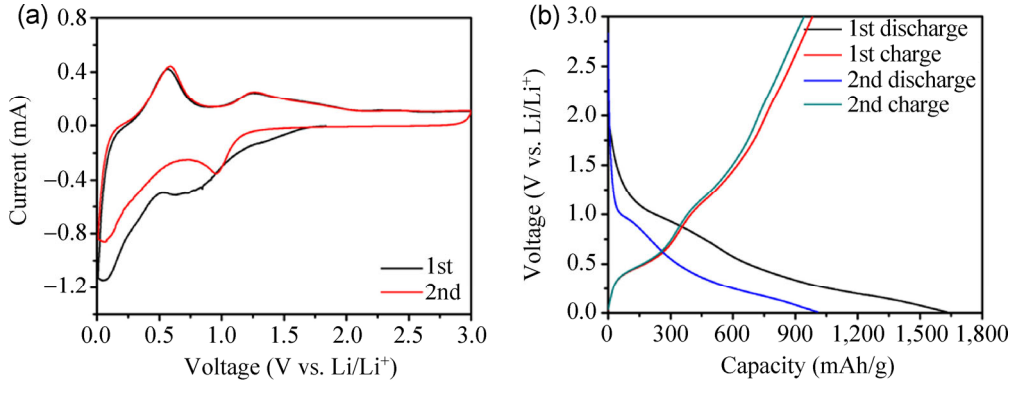

Figure 3 (a) Cyclic voltammograms of SnO_2–rGONRs at the scan rate of 0.4 mV/s in the potential range 0.01–3.0 V (vs. Li/Li^+). (b) The first two discharge–charge curves of SnO_2–rGONRs at a current density of 0.1 A/g in the potential range 0.01–3.0 V (vs. Li/Li^+).

of 0.1 A/g, the capacity of SnO_2–rGONRs was 942.8 mAh/g at the 2nd cycle. At the high current density of 3 A/g, the discharge capacity of SnO_2–rGONRs was ~640 mAh/g. When the current density was reduced back from 3.0 to 0.1 A/g, the value of the specific capacity at different current densities returned to its original value and then—at the same current density—increased as the cycle number increased. An increase in the capacity to 1,027 mAh/g at the 165th cycle was obtained at a current density of 0.1 A/g. This is a normal phenomenon for nanosized electrode materials in LIBs; many reports have demonstrated similar results [35]. One reason is that nanosized electrode materials have a high surface area in contact with the electrolyte. The formation of an electrolyte–electrode interface results in the observed increase in capacity.

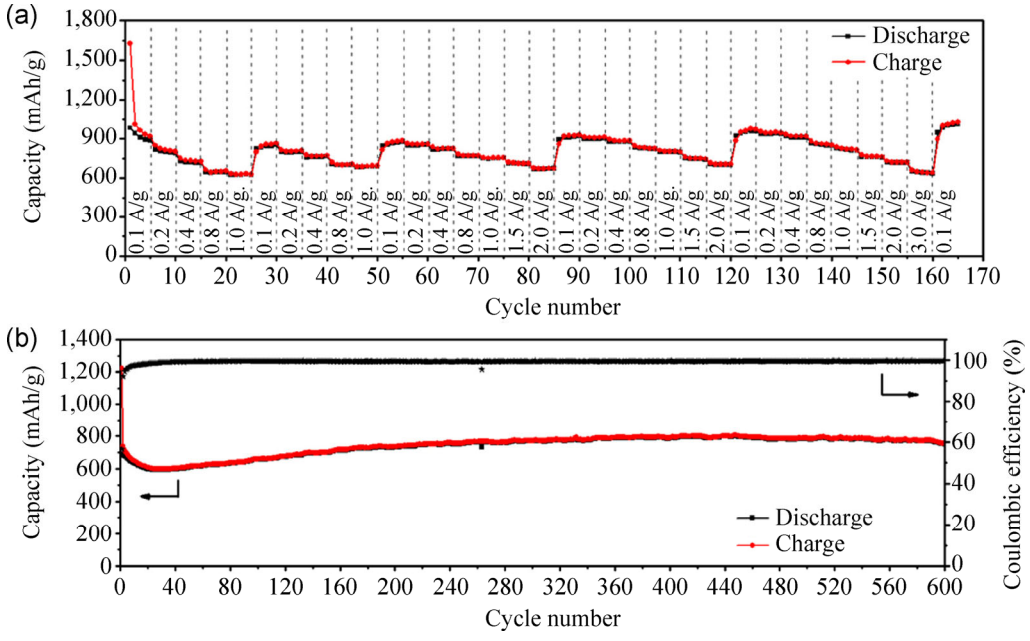

Figure 4 (a) Rate performance of SnO_2–rGONRs at various current rates from 0.1 to 3.0 A/g as a function of cycle number. (b) Cycling performance of SnO_2–rGONRs at 1.0 A/g.

Moreover, materials with high surface area can physically adsorb lithium ions during the discharging and charging processes. This also leads to the extra capacity in the LIBs. The decomposition of electrolyte and other side reactions also make contributions to the increase in the capacity.

These results demonstrate that SnO_2–rGONRs electrode materials have high capacity and good rate performance.

The cycling performance for SnO_2–rGONRs was also measured using discharge–charge repetition at a current density of 1.0 A/g as indicated in Fig. 4(b). The reversible discharge capacity of SnO_2–rGONRs was 737 mAh/g on its second cycle. The value dropped slowly to 598 mAh/g at the 30th cycle, but then increased in the following cycles and reached 806 mAh/g at the 448th cycle. The increase in the capacity in the later cycles indicates that the SnO_2–rGONRs materials might have an activation step. The electrolyte may not have been in contact with the inner regions of the SnO_2–rGONRs at first, thus taking some time for the electrolyte to flood the inner active materials. When contact was made because of the continued cycling, the SnO_2–rGONRs became fully electrochemically active, leading to the observed capacity increase. The material still maintained a high capacity and reached 753 mAh/g after 600 cycles. In addition, the coulombic efficiency of SnO_2–rGONRs remained at >99.5% (excluding the first few cycles). In contrast, the discharge capacity of pure SnO_2 was only 322 mAh/g at the 2nd cycle as shown in Fig. S4(a) (in the ESM). It also suffered serious capacity decay with less than 20% capacity retained after 40 cycles. Figure S4(b) (in the ESM) shows the poor cycling performance of rGONRs. Compared with its two components, SnO_2–rGONR materials demonstrate a greatly improved cycling performance in LIBs. The morphology of SnO_2–rGONRs after 200 discharge–charge cycles (SnO_2–rGONRs-200) (Figs. S5(a) and S5(b) in the ESM) is almost unchanged compared to the initial morphology of SnO_2–rGONRs shown in Figs. 1(a) and 1(b). The morphology of SnO_2–rGONRs-200 was also analyzed by TEM shown in Figs. S5(c) and S5(d) (in the ESM). The particles still had a good crystalline structure. Therefore, the design strategy worked well and resulted in good electrochemical performance in the LIBs.

Electrochemical impedance spectroscopy (EIS) was utilized to study the kinetic properties of the SnO_2–rGONRs. Figure 5(a) shows the Nyquist plots of the initial SnO_2–rGONRs and SnO_2–rGONRs-200. The insert is the enlarged part in the high frequency region. Figure 5(b) illustrates the equivalent circuit model. In

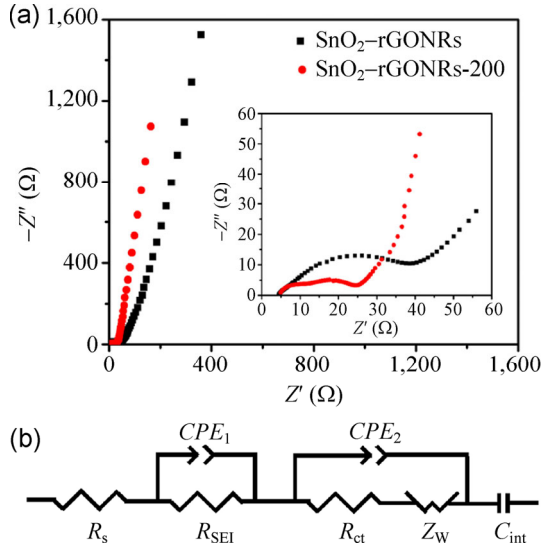

Figure 5 (a) Nyquist plots of SnO_2–rGONRs. The insert is the enlarged high frequency region. (b) The equivalent circuit that was used to fit the experimental data.

Fig. 5(b), R_s is the internal resistance of the tested battery, R_{SEI} and R_{ct} represent the SEI surface and charge-transfer resistance respectively, CPE_1 and CPE_2 are associated with the constant phase element and double layer capacitance across the surface respectively, Z_W is the Warburg resistance related to the lithium diffusion process, and C_{int} is the interaction capacitance [36, 37]. In Fig. 5(a), the inset plot of SnO_2–rGONRs-200 shows two semicircles in the high and intermediate frequency range and a sloping line with an angle ~45° to the real axis in the low frequency region. The two semicircles result from the Li^+ ion transport through the SEI film (R_{SEI}) and the interfacial charge transfer reaction (R_{ct}) combined with the constant phase element and the electrochemical double-layer capacitive behaviors CPE_1 and CPE_2, respectively. The sloping line is attributed to solid-state Li diffusion into the active materials (Z_W) [36]. The experimental Nyquist plots were modeled based on the equivalent circuit. The fitted impedance parameters are listed in Table S1 (in the ESM). The R_{SEI} of fresh SnO_2–rGONRs is 0.8 Ω and increases to 13.16 Ω for SnO_2–rGONRs-200. The stable SEI film is beneficial for the cycling stability of the electrodes [38]. Therefore, SnO_2–rGONRs demonstrate greatly improved LIBs cycling life. The R_{ct} of SnO_2–rGONRs decreases to 5.47 Ω after 200 cycles from 33.37 Ω for the fresh SnO_2–rGONRs. This change is consistent with the variation in rate performance and cycling performance of SnO_2–rGONRs.

3 Conclusion

We have successfully designed and synthesized nanostructured composites of SnO_2–rGONRs. In this composite, the nanosized SnO_2 particles formed directly on the rGONRs. Electrochemical experiments demonstrated that SnO_2–rGONRs exhibit high capacity, good rate performance, and excellent cycling stability as anode materials due to the synergic effect between the rGONRs and SnO_2. The composite SnO_2–rGONRs is effective in improving the electrochemical stability of the electrode materials for the lithium ion batteries.

Acknowledgements

The authors thank Sandia National Laboratory, the ONR MURI program (Nos. 00006766, and N00014-09-1-1066), the AFOSR MURI program (No. FA9550-12-1-0035), the AFOSR (No. FA9550-09-1-0581) and the Chinese Scholarship Council provided funding. The authors would also like to thank Celgard LLC for the kind donation of the battery separator material (Celgard 2300).

Electronic Supplementary Material: Supplementary material (detailed experimental procedures, morphology characterization, X-ray photoelectron spectroscopy, thermogravimetric analysis and additional electrochemical measurements) is available in the online version of this article at http://dx.doi.org/10.1007/s12274-014-0496-x.

References

[1] Su, Y. Z.; Li, S.; Wu, D. Q.; Zhang, F.; Liang, H. W.; Gao, P. F.; Cheng, C.; Feng, X. L. Two-dimensional carbon-coated graphene/metal oxide hybrids for enhanced lithium storage. *ACS Nano* **2012**, *6*, 8349–8356.

[2] Etacheri, V.; Marom, R.; Elazari, R.; Salitra, G.; Aurbach, D. Challenges in the development of advanced Li-ion batteries: A review. *Energy Environ. Sci.* **2011**, *4*, 3243–3262.

[3] Tarascon, J. M.; Armand, M. Issues and challenges facing rechargeable lithium batteries. *Nature* **2001**, *414*, 359–367.

[4] Wang, B.; Li, X. L.; Zhang, X. F.; Luo, B.; Jin, M. H.; Liang, M. H.; Dayeh, S. A.; Picraux, S. T.; Zhi, L. J. Adaptable silicon–carbon nanocables sandwiched between reduced graphene oxide sheets aslithium ion battery anodes. *ACS Nano* **2013**, *7*, 1437–1445.

[5] Aricò, A. S.; Bruce, P.; Scosati, B.; Tarascon, J. M. Nanostructured materials for advanced energy conversion and storage devices. *Nat. Mater.* **2005**, *4*, 366–377.

[6] Chen, J. S.; Lou, X. W. SnO_2-based nanomaterials: Synthesis and application in lithium-ion batteries. *Small* **2013**, *9*, 1877–1893.

[7] Haag, J. M.; Pattanaik, G.; Durstock, M. F. Nanostructured 3D electrode architectures for high-rate Li-ionbatteries. *Adv. Mater.* **2013**, *25*, 3238–3243.

[8] Zhang, L.; Zhang, G. Q.; Wu, H. B.; Yu, L.; Lou, X. W. Hierarchical tubular structures constructed by carbon-coated SnO_2 nanoplates for highly reversible lithium storage. *Adv. Mater.* **2013**, *25*, 2589–2593.

[9] Lou, X. W.; Li, C. M.; Archer, L. A. Designed synthesis of coaxial SnO_2@carbon hollow nanospheres for highly reversible lithium storage. *Adv. Mater.* **2009**, *21*, 2536–2539.

[10] Li, Y.; Zhu, S. M.; Liu, Q. L.; Gu, J. J.; Guo, Z. P.; Chen, Z. X.; Feng, C. L.; Zhang, D.; Moon, W. J. Carbon-coated SnO_2@C with hierarchically porous structures and graphite layers inside for a high-performance lithium-ion battery. *J. Mater. Chem.* **2012**, *22*, 2766–2773.

[11] He, M.; Yuan, L. X.; Hu, X. L.; Zhang, W. X.; Shu, J.; Huang, Y. H. A SnO_2@carbon nanocluster anode material with superior cyclability and rate capability for lithium-ion batteries. *Nanoscale* **2013**, *5*, 3298–3305.

[12] Wang, X.; Cao, X. Q.; Bourgeois, L.; Guan, H.; Chen, S.; Zhong, Y.; Tang, D. M.; Li, H. Q.; Zhai, T. Y.; Li, L. et al. N-doped graphene–SnO_2 sandwich paper for high-performance lithium-ion batteries. *Adv. Funct. Mater.* **2012**, *22*, 2682–2690.

[13] Yang, S.; Yue, W. B.; Zhu, J.; Ren, Y.; Yang, X. J. Graphene-based mesoporous SnO_2 with enhanced electrochemical performance for lithium-ion batteries. *Adv. Funct. Mater.* **2013**, *23* , 3570–3576.

[14] Zhou, X. S.; Yin, Y. X.; Wan, L. J.; Guo, Y. G. A robust composite of SnO_2 hollow nanospheres enwrapped by graphene as a high-capacity anode material for lithium-ion batteries. *J. Mater. Chem.* **2012**, *22*, 17456–17459.

[15] Ji, G.; Ding, B.; Sha, Z.; Wu, J. S.; Ma, Y.; Lee, J. Y. Conformal graphene encapsulation of tin oxide nanoparticle aggregates for improved performance in reversible Li^+ storage. *Nanoscale* **2013**, *5*, 5965–5972.

[16] Wang, L.; Wang, D.; Dong, Z. H.; Zhang, F. X.; Jin, J. Interface chemistry engineering for stable cycling of reduced GO/SnO_2 nanocomposites for lithium ion battery. *Nano Lett.* **2013**, *13*, 1711–1716.

[17] Wen, Z.; Wang, Q.; Zhang, Q.; Li, J. *In situ* growth of mesoporous SnO_2 on multiwalled carbon nanotubes: A novel composite with porous-tube structure as anode for lithium batteries. *Adv. Funct. Mater.* **2007**, *17*, 2772–2778.

[18] Ding, S. J.; Chen, J. S.; Lou, X. W. One-dimensional hierarchical structures composed of novel metal oxide nanosheets on a carbon nanotube backbone and their lithium-storage properties. *Adv. Funct. Mater.* **2011**, *21*, 4120–4125.

[19] Hu, R. Z.; Sun, W.; Liu, H.; Zeng, M. Q.; Zhu, M. The fast filling of nano-SnO_2 in CNTs by vacuum absorption: A new approach to realize cyclic durable anodes for lithium ion batteries. *Nanoscale* **2013**, *5*, 11971–11979.

[20] Lin, J.; Peng, Z. W.; Xiang, C. S.; Ruan, G. D.; Yan, Z.; Natelson, D.; Tour, J. M. Graphene nanoribbon and nano-structured SnO_2 composite anodes for lithium ion batteries. *ACS Nano* **2013**, *7*, 6001–6006.

[21] Ye, J. F.; Zhang, H. J.; Yang, R.; Li, X. G.; Qi, L. M. Morphology-controlled synthesis of SnO_2 nanotubes by using 1D silica mesostructures as sacrificial templates and their applications in lithium-ion batteries. *Small* **2010**, *6*, 296–306.

[22] Wang, Y.; Lee, J. Y.; Zeng, H. C. Polycrystalline SnO_2 nanotubes prepared via infiltration casting of nanocrystallites and their electrochemical application. *Chem. Mater.* **2005**, *17*, 3899–3903.

[23] Park, M. S.; Wang, G. X.; Kang, Y. M.; Wexler, D.; Dou, S. X.; Liu, H. K. Preparation and electrochemical properties of SnO_2 nanowires for application in lithium-ion batteries. *Angew. Chem. Int. Edit.* **2007**, *119*, 764–767.

[24] Wang, C.; Zhou, Y.; Ge, M. Y.; Xu, X. B.; Zhang, Z. L.; Jiang, J. Z. Large-scale synthesis of SnO_2 nanosheets with high lithium storage capacity. *J. Am. Chem. Soc.* **2010**, *132*, 46–47.

[25] Reddy, M. V.; Subba Rao, G. V.; Chowdari, B. V. R. Metal oxides and oxysalts as anode materials for Li ion batteries. *Chem. Rev.* **2013**, *113*, 5364–5457.

[26] Deng, J. W.; Yan, C. L.; Yang, L. C.; Baunack, S.; Oswald, S.; Wendrock, H.; Mei, Y. F.; Schmidt, O. G. Sandwich-stacked SnO_2/Cu hybrid nanosheets as multichannel anodes for lithium ion batteries. *ACS Nano* **2013**, *7*, 6948–6954.

[27] Zhou, W. W.; Cheng, C. W.; Liu, J. P.; Tay, Y. Y.; Jiang, J.; Jia, X. T.; Zhang, J. X.; Gong, H.; Hng, H. H.; Yu, T. et al. Lithium-ion batteries: Epitaxial growth of branched α-Fe_2O_3/SnO_2 nano-heterostructures with improved lithium-ion battery performance. *Adv. Funct. Mater.* **2011**, *21*, 2439–2445.

[28] Wang, Y. L.; Xu, J. J.; Wu, H.; Xu, M.; Peng, Z. P.; Zheng, G. F. Hierarchical SnO_2–Fe_2O_3 heterostructures as lithium-ion battery anodes. *J. Mater. Chem.* **2012**, *22*, 21923–21927.

[29] Higginbotham, A. L.; Kosynkin, D. V.; Sinitskii, A.; Sun, Z. Z.; Tour, J. M. Lower-defect graphene oxide nanoribbons from multiwalled carbon nanotubes. *ACS Nano* **2010**, *4*, 2059–2069.

[30] Liu, B.; Chia, Z. W.; Lee, Z. Y.; Cheng, C. H.; Lee, J. Y.; Liu, Z. L. The importance of water in the polyol synthesis

of carbon supported platinum–tin oxide catalysts for ethanol electrooxidation. *J. Power Sources* **2012**, *206*, 97–102.

[31] Li, D.; Müller, M. B.; Gilje, S.; Kaner, R. B.; Wallace, G. G. Processable aqueous dispersions of graphene nanosheets. *Nat. Nanotechnol.* **2008**, *3*, 101–105.

[32] Campos-Delgado, J.; Romo-Herrera, J. M.; Jia, X. T.; Cullen, D. A.; Muramatsu, H.; Kim, Y. A.; Hayashi, T.; Ren, Z. F.; Smith, D. J.; Okuno, Y. et al. Bulk production of a new form of sp^2 carbon: Crystalline graphene nanoribbons. *Nano Lett.* **2008**, *8*, 2773–2778.

[33] Utsumi, S.; Honda, H.; Hattori, Y.; Kanoh, H.; Takahashi, K.; Sakai, H.; Abe, M.; Yudasaka, M.; Iijima, S.; Kaneko, K. Direct evidence on C–C single bonding in single-wall carbon nanohorn aggregates. *J. Phys. Chem. C* **2007**, *111*, 5572–5575.

[34] Jiang, Y. Z.; Yuan, T. Z.; Sun, W. P.; Yan, M. Electrostatic spray deposition of porous SnO_2/graphene anode films and their enhanced lithium-storage properties. *ACS Appl. Mater. Interfaces* **2012**, *4*, 6216–6220.

[35] Reddy, M. V.; Subba Rao, G. V.; Chowdari, B. V. R. Metal oxides and oxysalts as anode materials for Li ion batteries. *Chem. Rev.* **2013**, *113*, 5364–5457.

[36] Qian, D. N.; Xu, B.; Cho, H. M.; Hatsukade, T.; Carroll, K. J.; Meng, Y. S. Lithium lanthanum titanium oxides: A fast ionic conductive coating for lithium-ion battery cathodes. *Chem. Mater.* **2012**, *24*, 2744–2751.

[37] Chang, K.; Chen, W. X. L-cysteine-assisted synthesis of layered MoS_2/graphene composites with excellent electrochemical performances for lithium ion batteries. *ACS Nano* **2011**, *5*, 4720–4728.

[38] Verma, P.; Maire, P.; Novák, P. A review of the features and analyses of the solid electrolyte interphase in Li-ion batteries. *Electrochim. Acta* **2010**, *55*, 6332–6341.